A novel systems biology approach to evaluate mouse models of late-onset Alzheimer's disease

Christoph Preuss[1*], Ravi Pandey[1*], Erin Piazza[2], Alexander Fine[1], Asli Uyar[1], Thanneer Perumal[2], Dylan Garceau[1], Kevin P Kotredes[1], Harriet Williams[1], Lara M Mangravite [3], Bruce T. Lamb[4], Adrian L. Oblak[4], Gareth R. Howell[1], Michael Sasner[1], Benjamin A Logsdon[3], Gregory W. Carter[1]†

[1] The Jackson Laboratory, Bar Harbor, ME, USA.

[2] NanoString, Seattle, WA, USA.

[3] Sage Bionetworks, Seattle, WA, USA.

[4] Stark Neurosciences Research Institute, Indiana University School of Medicine, Indianapolis, IN 46202 USA

* These authors contributed equally to the work

Keywords: Alzheimer's disease, gene expression, co-expression modules, mouse models, reproducibility

†Correspondence:

Gregory Carter, Ph.D.

The Jackson Laboratory

600 Main Street

04609 Bar Harbor, Maine

Phone: (207)-288-6025

Email: Gregory.Carter@jax.org

Word count: 4058

Keywords: Alzheimer, Transcriptome, Mouse, Co-expression network analysis, RNAseq

ABSTRACT

Background: Late-onset Alzheimer's disease (LOAD) is the most common form of dementia worldwide. To date, animal models of Alzheimer's have focused on rare familial mutations, due to a lack of frank neuropathology from models based on common disease genes. Recent multi-cohort studies of postmortem human brain transcriptomes have identified a set of 30 gene co-expression modules associated with LOAD, providing a molecular catalog of relevant endophenotypes. **Results:** This resource enables precise gene-based alignment between new animal models and human molecular signatures of disease. Here, we describe a new resource to efficiently screen mouse models for LOAD relevance. A new NanoString nCounter® Mouse AD panel was designed to correlate key human disease processes and pathways with mRNA from mouse brains. Analysis of three mouse models based on LOAD genetics, carrying APOE4 and TREM2*R47H alleles, demonstrated overlaps with distinct human AD modules that, in turn, are functionally enriched in key disease-associated pathways. Comprehensive comparison with full transcriptome data from same-sample RNA-Seq shows strong correlation between gene expression changes independent of experimental platform. **Conclusions:** Taken together, we show that the nCounter Mouse AD panel offers a rapid, cost-effective and highly reproducible approach to assess disease relevance of potential LOAD mouse models.

BACKGROUND

Late-onset Alzheimer's disease (LOAD) is the most common cause of dementia worldwide (1). LOAD presents as a heterogenous disease with highly variable outcomes. Recent efforts have been made to molecularly characterize LOAD using large cohorts of post-mortem human brain transcriptomic data (2). Systems-level analysis of these large human data sets has revealed key drivers and molecular pathways that reflect specific changes resulting from disease (2,3). These studies have been primarily driven by gene co-expression analyses that reduce transcriptomes to modules representing specific disease processes or cell types across heterogenous tissue samples (2,4,5). Similar approaches have been used to characterize mouse models of neurodegenerative disease (6). Detailed cross-species analysis reveals a translational gap between animal models and human disease, as no existing models fully recapitulate pathologies associated with LOAD (7,8). New platforms to rapidly assess the translational relevance of new animal models of LOAD will allow efficient identification of the most promising preclinical models.

In this study, we describe a novel gene expression panel to assess LOAD-relevance of mouse models based on expression of key genes in the brain. We used a recent human molecular disease catalog based on harmonized co-expression data from three independent post mortem brain cohorts (ROSMAP, Mayo, Mount Sinai Brain bank) (9–11) and seven brain regions that define 30 human co-expression modules and five consensus clusters derived from the overlap of those modules (12). These modules were used to design a mouse gene expression panel to assess the molecular overlap between human disease states and mouse models. This nCounter Mouse AD panel

was piloted with samples from three novel mouse models of LOAD. Same-sample comparison between NanoString and RNA-Seq data demonstrated high per-gene correlation and overall concordance when separately compared to human disease co-expression modules. Taken together, the rapid screening of mouse models in the course of different life stages will allow better characterization of models based on alignment with specific human molecular pathologies.

RESULTS

Human-mouse co-expression module conservation and probe coverage across 30 LOAD associated modules

An overview of the Mouse AD panel design for translating the 30 human AMP-AD co-expression modules from three cohorts and seven brain regions is depicted in Figure 1. Mouse to human gene prioritization resulted in the selection of 760 key mouse genes targeting a subset of highly co-expressed human genes plus 10 housekeeping genes, which explained a significant proportion of the observed variance across the 30 human AMP-AD modules (Methods). Co-expression modules were grouped into functionally distinct consensus clusters as previously described by Logsdon, et al (see also Supplemental Table 1) (12). These consensus clusters contain expression modules from different brain regions and independent studies that share a high overlap in gene content and similar expression characteristics. Consensus clusters were annotated based on Reactome pathway enrichment analysis for the corresponding genes within each functionally distinct cluster (Methods, Supplemental Table 1). Since consensus clusters showed an enrichment of multiple biological pathways, the highest rank and

non-overlapping Reactome pathway was used to refer to each cluster (Supplemental Table 2). In order to assess the conservation of sequence and gene expression levels between human and mouse genes for each of the 30 human co-expression modules, dN/dS values were correlated with the overall overlap in expression in brains from six-month-old C57BL/6J (B6) mice (Figure 2A). The fraction of orthologous genes expressed in the mouse brain, based on the presence or absence of transcripts at detectable levels, was very highly correlated with the overall module conservation (p-value < 2.2e-16, Pearson's correlation coefficient: -0.96). Module conservation was based on the median dN/dS statistics measuring the rate of divergence in the coding sequence for all genes within a given module between both species (Figure S1). Notably, human co-expression modules of Consensus Cluster C, associated with the neuronal system and neurotransmission, showed the lowest degree of sequence divergence with a high proportion of human genes (64-72%) expressed in six-month-old B6 mice. In contrast to the highly conserved neuronal modules, immune modules of Consensus Cluster B contained genes that recently diverged on the sequence level and acquired a higher number of destabilizing missense variants. These modules showed the highest median dN/dS values and the lowest fraction of genes (27-46%) expressed in the mouse brain across all tested modules. The remaining human co-expression modules, associated with different functional categories (Figure 2A, Supplemental Table 1), had intermediate overlap in expression levels between human and mice. Each of the 30 human co-expression modules was covered with an average of 148 NanoString mouse probes (SD = 50 probes), where a single mouse probe can map to multiple human modules from different study cohorts and across several brain regions. Overall,

mouse probe coverage for human co-expression modules ranged between 4% and 19%, depending on the size and level of conservation of the targeted human module (Figures 2B and 2C, Supplemental Tables S2 and S3). For three of the largest human co-expression modules harboring over 4,000 transcripts, the probe coverage was slightly below the targeted 5% coverage threshold. However, these large modules are predominantly associated with neuronal function and show a high degree of expression and sequence conservation between human and mouse (Figures 2A). Immune modules, containing genes that recently diverged on the coding sequence level, are well covered with a median coverage of 10% (Figure 2C). A complete annotation of mouse probes to human transcripts for each human co-expression module is provided in Supplemental Table S3. In addition, we compared our novel panel to the existing nCounter Mouse Neuropathology panel designed to assess expression changes in multiple neurodegenerative diseases. We observed an overlap of 105 probes (7%) between both panels, highlighting that most of our selected probe content is novel and specific to LOAD associated disease processes and pathways.

Prioritized subset of key genes show a higher degree of sequence conservation and expression level across modules

In order to assess the level of sequence divergence and expression for the prioritized subset of genes on the novel panel, the selected subset of genes were compared to all genes across the 30 human co-expression modules. The 760 key genes, explaining a significant proportion of the observed variance in each human module, showed an overall lower level of sequence divergence (median dN/dS values) when compared to all other genes in the modules (Figure 3, Figure S1). Furthermore, the selected key

144 genes on the Mouse AD panel also displayed a higher average level of gene expression
145 in brains of six-month-old B6 mice compared to the remaining genes for each of the 30
146 modules (Figure 3). This highlights that our formal prioritization procedure resulted in
147 the selection of a subset of highly expressed key genes, which are also more conserved
148 between human and mouse facilitating the translation of co-expression profiles across
149 species.

150 *Novel mouse models harboring LOAD associated risk variants correlate with distinct*
151 *AMP-AD modules in a brain region- and pathway-specific manner*

152 Three novel mouse models, harboring two LOAD risk alleles, (Supplemental Table S4)
153 were used to translate co-expression profiles between human and mouse brain
154 transcriptome data using our novel Mouse AD panel. Transcriptome analysis was
155 performed for the APOE4 KI mouse, carrying a humanized version of the strongest
156 LOAD associated risk allele (*APOE-ε4*) and the Trem2*R47H mouse, which harbors a
157 rare deleterious variant in *TREM2*. The rare *TREM2* R47H missense variant
158 (rs75932628) has been previously associated with LOAD in multiple independent
159 studies [16,17]. In addition, a mouse model harboring both, the common and rare AD
160 risk variants (APOE4 KI/Trem2*R47H) was used to compare the transcriptional effects
161 in mice carrying both variants to mice carrying only a single risk allele and B6 controls.
162 Mouse transcriptome data for half brains was analyzed at different ages (4-14 months)
163 to estimate the overlap with human post-mortem co-expression modules during aging.
164 We observed specific overlaps with distinct disease processes and molecular pathways
165 at different ages for the APOE4 KI and Trem2*R47H mouse models. At an early age (2-
166 5 months), male APOE4 KI and Trem2*R47H mice showed strong positive correlations

(p-value < 0.05, Pearson's correlation coefficient < -0.3) with human co-expression modules in Consensus Cluster E that are enriched for transcripts associated with cell cycle and RNA non-mediated decay pathways in multiple brain regions (Figure 4). Furthermore, Trem2*R47H male mice showed a significantly negative association (p-value < 0.05, Pearson's correlation coefficient < -0.2) with immune related human modules in the superiortemporal gyrus, the inferiorfrontal gyrus, cerebellum and prefrontal cortex (Figure 4). This effect becomes more pronounced later in development, between six and 14 months, when the correlation with human immune modules is also observed in Trem2*R47H female mice. During mid-life, (6-9 month-old age group), we observed an age-dependent effect for the APOE4 KI mouse in which human neuronal modules in Consensus Cluster C start to become positively correlated with the corresponding human expression modules (Figure 4). Interestingly, neuronal co-expression modules which are associated with synaptic signaling appear to be positively correlated with APOE4 KI, but not Trem2*R47H mice in an age dependent manner. This up-regulation of genes associated with synaptic signaling and a decrease of transcripts enriched for cell cycle, RNA non-mediated decay, myelination and glial development in aged mice was consistent for multiple brain regions and across three independent human AD cohorts. When compared to APOE4 KI mice, Trem2*R47H mice showed an age dependent decrease in genes associated with the immune response in several AMP-AD modules which is not observed for APOE4 KI mice (Figure 4). Notably, the APOE4 KI/Trem2*R47H mice showed characteristics of both single variant mouse models. At an early age, an overlap with both neuronal and immune associated human modules is observed and becomes more pronounced during aging.

Comparison between nCounter Mouse AD panel and RNA-Seq data

To assess the validity of the novel Mouse AD panel across transcriptomic platforms, we compared the results from the nCounter analysis to results from RNA-Seq data for the same 137 mouse brain samples. A correlation analysis was performed to compare the expression of the 770 NanoString probes across co-expression modules with RNA-Seq transcript expression for all ages (3-5, 7-9, 12-14 months), highlighting the different LOAD mouse models as independent variables (Figure 5). For the direct comparison, between the 770 NanoString probes with corresponding RNA-Seq transcripts, a similar range of correlation coefficients between human data and the three mouse models was observed (Figure 5A). Overall, the correlation between the RNA-Seq and NanoString platforms were high across all age groups (Pearson's correlation coefficients: 0.65-0.69) when comparing the subset of 760 key transcripts and 10 housekeeping transcripts across platforms. This demonstrates that the novel NanoString panel, despite the limited number of key custom probes, can achieve similar results when compared to high-throughput RNA-Seq data. Furthermore, the alignment of human and mouse modules based on the expression of all genes within each modules showed a weaker range of correlations when compared to transcripts covered by the 770 NanoString probes (Figure 5B). Notably, we observed an age specific effect in which the correlation between nCounter probe expression and RNA-Seq transcripts increased over time (Figure 5B). A mild correlation at around three months of age (Pearson's correlation coefficient: 0.39) increased to a moderate correlation at 12 months of age (Pearson's correlation coefficient: 0.51). Furthermore, we observed a high correlation of log count values for the majority of NanoString probes when compared to log TPM transcript

ratios from RNA-Seq data. The majority of the 770 measured NanoString probes (716/770 probes, 93%) were positively correlated with RNA-Seq transcripts (Figure S2). In order to test whether noise introduced by highly variable transcripts affects the correlation between NanoString probes and RNA-Seq transcripts, Pearson's correlation coefficients and variance in RNA-Seq expression across 137 samples were compared. There was no significant trend indicating an effect of highly variable transcripts on the overall correlation coefficients between transcripts measured by RNA-Seq and NanoString (Figure S2).

DISCUSSION

Here, we describe a novel systems biology approach to rapidly assess disease relevance for three novel mouse models carrying two human risk variants, strongly associated with LOAD. The nCounter Mouse AD gene expression panel was designed to align human brain transcriptome data covering 30 co-expression modules. Cross-species comparison of human and mouse revealed that immune associated co-expression modules which harbor genes that have recently diverged in sequence were more likely to be lowly expressed or absent at the transcript level in brains from 6 month old B6 mice. In contrast, neuronal modules containing genes with a lower degree of sequence divergence between both species were more likely to be highly and constitutively expressed in the mouse brain when compared to the remaining co-expression modules. This is in line with evidence from multiple studies highlighting that conserved neuronal process in the brain are under strong purifying selection while immune related genes are more likely to diverge in function and expression patterns across species (13,14). By using our prioritization approach, we selected for 760 key

mouse genes targeting a subset of highly co-expressed human genes. This subset of genes on the NanoString panel showed overall lower levels of sequence divergence compared to human genes and higher expression levels in the mouse brain, reducing potential noise introduced by lowly expressed transcripts across expression modules.

Furthermore, we observed a robust and significant correlation between human co-expression modules and three mouse models carrying two LOAD associated risk variants (APOE4 KI, Trem2*R47H, APOE4 KI/Trem2*R47H). Cross-platform comparison between the novel Mouse AD panel and RNA-Seq data revealed a strong correlation between mouse gene expression changes independent of platform related effects. Notably, the correlation between nCounter probe and RNA-Seq transcript expression with human co-expression modules was highest in aged mice older than 12 months. This age-dependent overlap might be expected due to the late-onset nature of Alzheimer's disease resulting in an increased number of highly co-expressed genes in aged mice carrying human LOAD risk variants. In addition, the strongest correlation between human and mouse module signatures was observed when using the subset of 770 transcripts on the NanoString panel. This highlights that assessment of key genes in the brain, contributing highly to module expression, can improve the characterization of novel LOAD mouse models and their alignment with specific human co-expression modules.

Interestingly, novel LOAD mouse models showed better concordance with distinct human co-expression modules, reflecting a different transcriptional response driven by the human *APOE* and *TREM2* associated LOAD risk variants. The strong negative correlation between the Trem2*R47H knock-in mice and immune related human co-

expression highlights the important role of the LOAD associated *TREM2* R47H variant in Alzheimer's related immune processes. This effect is reproducible across human co-expression modules, which derive from three independent cohorts and five different brain regions (cerebellum, frontal cortex, temporal gyrus, frontal gyrus, frontal pole). Similarly, a strong negative correlation between co-expression modules associated with cell cycle and DNA repair was observed for the mouse APOE4 KI model. This overlap with human late-onset co-expression signatures early in life was observed for a number of different brain regions and is absent in Trem2*R47H knock-in mice. Furthermore, aged APOE4 KI mice show a strong overlap with several human neuronal co-expression modules enriched for genes that play an important role in synaptic signaling and myelination. Although, APOE4 KI mice lack a clear neurodegenerative phenotype, this age dependent shift in co-expression patterns associated with core LOAD pathologies points to an increased susceptibility of cognitive decline in aged mice. This is in line with several studies, which have shown that cognitive deficits in APOE4 transgenic mice develop late in life (15,16).

Limitations of the approach

Albeit being an excellent resource for characterizing molecular pathways and key drivers of disease, co-expression modules based on human post-mortem brain data have several limitations. They might not reflect changes that occur early in disease pathogenesis. In addition, although a high concordance was observed across brain regions for the 30 modules, they might not cover individual or region-specific differences in patients in response to amyloid and tau pathology (12). Furthermore, we used brain homogenates from our mouse models for the transcript comparison with different

human brain regions in this study. Dissection of mouse brain regions to match the human studies might further improve the observed co-expression module correlations.

CONCLUSIONS

Taken together, we show that the novel nCounter Mouse AD gene expression panel offers a rapid and cost-effective approach to assess disease relevance of novel LOAD mouse models. Furthermore, this co-expression based approach offers a high level of reproducibility and will supplement methods solely based on differential expression analysis. Ultimately, this will help us to better understand the relevance of novel LOAD mouse models in regard to specific pathways and processes contributing to late-onset Alzheimer's disease.

METHODS

AMP-AD post-mortem brain cohorts and gene co-expression modules

Data on the 30 human AMP-AD co-expression modules was obtained from the Synapse data repository (DOI: 10.7303/syn11932957.1). The modules derive from three independent LOAD cohorts, including 700 samples from the ROSMAP cohort, 300 samples from the Mount Sinai Brain bank and 270 samples from the Mayo cohort. Details on post-mortem brain sample collection, tissue and RNA preparation, sequencing, and sample QC can be found in previously published work related to each cohort (10,11,17). A detailed description on how co-expression modules were identified can be found in the recent study that identified the harmonized human co-expression modules as part of transcriptome wide AD meta-analysis (12). Briefly, Logsdon et al. performed library normalization and covariate adjustments for each human study

separately using fixed/mixed effects modeling to account for batch effects. Among the 2,978 AMP-AD modules identified across all tissues (10.7303/syn10309369.1), 660 modules were selected by Logsdon et al. which showed an enrichment for at least one AD-specific differential expressed gene set from the meta-analysis (10.7303/syn11914606) in cases compared to controls. Lastly, the edge betweenness graph clustering method was applied to identify 30 aggregate modules that are not only differentially expressed but are also replicated across multiple independent co-expression module algorithms (12). Among the 30 aggregate co-expression modules, five consensus clusters have been described by Logsdon et al. (12). These consensus clusters consist of a subset of modules which are associated with similar AD related changes across the multiple studies and brain regions. Here, we used Reactome pathway (https://reactome.org/) enrichment analysis to identify specific biological themes across these five consensus clusters. A hypergeometric model, implemented in the clusterProfiler R package (18), was used to assess whether the number of selected genes associated within each set of AMP-AD modules defining a consensus cluster was larger than expected. All p-values were calculated based the hypergeometric model (19). Pathways were ranked based on their Bonferroni corrected p-values to account for multiple testing. Finally, consensus clusters were annotated based on the highest ranked and non-overlapping term for each functionally distinct cluster.

Selection of NanoString probes for the nCounter Mouse AD Panel

Since NanoString gene expression panels are comprised of 770 probes with the option to customize 30 additional probes, we developed a formal prioritization procedure to identify the most representative genes and ensure broadest coverage across all

modules (Figure 1). Expression and transcript annotations for the 30 human co-expression modules were obtained via the AMP-AD knowledge portal (www.synapse.org/#!Synapse:syn11870970/tables/). To prioritize probe targets for the novel Mouse AD panel, human genes were ranked within each of the human AMP-AD co-expression modules based on their percentage of variation explaining the overall module behavior. First, we calculated a gene ranking score by multiplying correlations of transcripts with the percentage of variation explained by the first five principal components within each of the aggregated human AMP-AD modules. Secondly, the sums of the resulting gene scores for the first five principal components were calculated and converted to absolute values in order to rank highly positive or negative correlated transcripts within each human co-expression module. As a next step, only human transcripts with corresponding one-to-one mouse orthologous genes that are expressed in whole-brain tissue samples from six-month-old B6 mice were retained for downstream prioritization. Furthermore, we included information on drug targets for LOAD from the AMP-AD Agora platform (agora.ampadportal.org), as nominated by members of the AMP-AD consortium (10.7303/syn2580853). A total of 30 AMP-AD drug discovery targets that were highly ranked in our gene ranking approach and nominated by multiple AMP-AD groups were included on the panel (Supplemental Table 3). Finally, ten housekeeping genes (*AARS, ASB7, CCDC127, CNOT10, CSNK2A2, FAM104A, LARS, MTO1, SUPT7L, TADA2B*) were included on the panel as internal standard references for probe normalization. This resulted in a total of 770 proposed NanoString probes, targeting the top 5% of ranked genes for each human AMP-AD expression module.

350 *nCounter Mouse AD Panel Probe Design*

351 The probe design process breaks a transcript's sequence down into 100 nucleotide (nt)
352 windows to profile for probe characteristics, with the final goal of choosing the optimal
353 pair of adjacent probes to profile any given target. Each window is profiled for intrinsic
354 sequence makeup – non-canonical bases, G/C content, inverted and direct repeat
355 regions, runs of poly-nucleotides, as well as the predicted melting temperature (Tm) for
356 each potential probe-to-target interaction. The window is then divided in half to
357 generate a probe pair, wherein each probe is thermodynamically tuned to determine the
358 optimal probe length (ranging in size from 35-50 nt) within the 100 nt target region.
359 Next, a cross-hybridization score is calculated for each probe region, using BLAST (20)
360 to identify potential off-target interactions. In addition to a cross-hybridization score, a
361 splice isoform coverage score was generated to identify transcripts that are isoforms of
362 the gene intended to be targeted by the probe in question. Once all of this information is
363 compiled, the final probe is then selected by identifying the candidate with the optimal
364 splice form coverage, cross-hybridization score, and thermodynamic profile.

365 *In-silico panel QC for intramolecular interactions*

366 To ensure that there are no potential intramolecular probe-probe interactions that could
367 cause elevated background for any individual probe pair, a stringent intermolecular
368 screen is run on every collection of probes assembled into a panel. A sensitive
369 algorithm was used that calculates both the Tm and the free energy potential of
370 interactions between every possible pair of probes in the project. If two probes conflict in
371 a way that would likely cause background based on this calculation, an alternative

probe is selected for one of the targets and the screening is re-run until there are no known conflicts.

Mouse models

All experiments involving mice (Supplemental Table S4) were conducted in accordance with policies and procedures described in the Guide for the Care and Use of Laboratory Animals of the National Institutes of Health and were approved by the Institutional Animal Care and Use Committee at The Jackson Laboratory. All mice were bred and housed in a 12/12 hour light/dark cycle. All experiments were performed on a unified genetic background (C57BL/6J).

Mouse brain sample collection

Upon arrival at the terminal endpoint for each aged mouse cohort, individual animals were weighed prior to intraperitoneal administration of ketamine (100mg/kg) and xylazine (10mg/kg). First confirming deep anesthetization via toe pinch, an incision was made along the midline to expose the thorax and abdomen followed by removal of the lateral borders of the diaphragm and ribcage revealed the heart. A small cut was placed in the right atrium to relieve pressure from the vascular system before transcardially perfusing the animal with 1XPBS via injection into the left ventricle. With the vascular system cleared, the entire brain was carefully removed and weighed before hemisecting along the midsagittal plane. Hemispheres were immediately placed in a cryovial and snap-frozen on dry ice. Brain samples were stored at -80°C until RNA extraction was performed.

RNA sample preparation

RNA was isolated from tissue using the MagMAX mirVana Total RNA Isolation Kit (ThermoFisher) and the KingFisher Flex purification system (ThermoFisher, Waltham, MA). Brain hemispheres were thawed to 0°C and were lysed and homogenized in TRIzol Reagent (ThermoFisher). After the addition of chloroform, the RNA-containing aqueous layer was removed for RNA isolation according to the manufacturer's protocol, beginning with the RNA bead binding step. RNA concentration and quality were assessed using the Nanodrop 2000 spectrophotometer (Thermo Scientific) and the RNA Total RNA Nano assay (Agilent Technologies, Santa Clara, CA).

RNAseq library preparation and data collection

Sequencing libraries were constructed using TruSeq DNA V2 (Illumina, San Diego, CA) sample prep kits and quantified using qPCR (Kapa Biosystems, Wilmington, MA). The mRNA was fragmented, and double-stranded cDNA was generated by random priming. The ends of the fragmented DNA were converted into phosphorylated blunt ends. An 'A' base was added to the 3' ends. Illumina®-specific adaptors were ligated to the DNA fragments. Using magnetic bead technology, the ligated fragments were size-selected and then a final PCR was performed to enrich the adapter-modified DNA fragments, since only the DNA fragments with adaptors at both ends will amplify. Libraries were pooled and sequenced by the Genome Technologies core facility at The Jackson Laboratory. Samples were sequenced on Illumina HiSeq 4000 using HiSeq 3000/4000 SBS Kit reagents (Illumina), targeting 30 million read pairs per sample. Samples were split across multiple lanes when being run on the Illumina HiSeq, once the data was received the samples were concatenated to have a single file for paired-end analysis.

NanoString gene expression panel and data collection

The NanoString Mouse AD gene expression panel was used for gene expression profiling on the nCounter platform (NanoString, Seattle, WA) as described by the manufacturer. nSolver software was used for analysis of NanoString gene expression values.

Normalization of NanoString data

Normalization was done by dividing counts within a lane by geometric mean of the housekeeping genes from the same lane. For the downstream analysis, counts were log-transformed from normalized count values.

Mouse-human expression comparison

First, we performed differential gene expression analysis for each mouse model and sex using the voom-limma (21) package in R. Secondly, we computed correlation between changes in expression (log fold change) for each gene in a given module with each mouse model, sex and age. Correlation coefficients were computed using cor.test function built in R as:

$$\text{cor.test}(\ \text{LogFC(h)}, \text{LogFC(m)}\ ) \qquad (1)$$

where LogFC(h) is the log fold change in transcript expression of human AD patients compared to control patients and LogFC(m) is the log fold change in expression of mouse transcripts compare to control mouse models. LogFC values for human transcripts were obtained via the AMP-AD knowledge portal (https://www.synapse.org/#!Synapse:syn11180450).

438 *Quality control of RNA-Seq data and read alignment*

439 Sequence quality of reads was assessed using FastQC (v0.11.3, Babraham). Low-
440 quality bases were trimmed from sequencing reads using Trimmomatic (v0.33) (22).
441 After trimming, reads of length longer than 36 bases were retained. The average quality
442 score at each base position was greater than 30 and sequencing depth were in range of
443 60 – 120 million reads. All RNA-Seq samples were mapped to the mouse genome
444 (mm10 reference, build 38, ENSEMBL) using ultrafast RNA-Seq aligner STAR (23)
445 (v2.5.3). The genes annotated for mm10 (GRCm38) were quantified in two ways:
446 Transcripts per million (TPM) using RSEM (v1.2.31) and raw read counts using HTSeq-
447 count (v0.8.0).

448 *Mouse-human co-expression module conservation*

449 Genomic information on orthologous groups was obtained via the latest ENSEMBL build
450 for human genome version GRCh38. All orthologous relationships were downloaded via
451 BioMart (24) (biomart.org). dN/dS statistics were retrieved for all orthologous gene pairs
452 with a one-to-one relationship between human and mouse. dN/dS values are calculated
453 as the ratio of nonsynonymous substitutions to the number of synonymous substitutions
454 in protein coding genes. The dN/dS values in ENSEMBL were calculated based on the
455 latest version of the codeml (http://abacus.gene.ucl.ac.uk/software/paml.html) package
456 using standard parameters (ensembl.org/info/genome/compara/homology_method.html)
457 (25).

458

DECLARATIONS

Acknowledgments

We thank the many institutions and their staff that provided support for this study and who were involved in this collaboration. We would like to acknowledge Jamie Kuhar for her critically reading of the manuscript.

Funding

This study was supported by the National Institutes of Health grant U54 AG 054354.

Availability of data and materials

The results published here are in whole or in part based on data obtained from the AMP-AD Knowledge Portal (doi:10.7303/syn2580853). ROSMAP Study data were provided by the Rush Alzheimer's Disease Center, Rush University Medical Center, Chicago. Data collection was supported through funding by NIA grants P30AG10161, R01AG15819, R01AG17917, R01AG30146, R01AG36836, U01AG32984, U01AG46152, the Illinois Department of Public Health, and the Translational Genomics Research Institute. Mayo RNAseq Study data were provided by the following sources: The Mayo ClinicAlzheimer's Disease Genetic Studies, led by Dr. Nilufer Ertekin-Taner and Dr. Steven G. Younkin, Mayo Clinic, Jacksonville, FL using samples from the Mayo Clinic Study of Aging, the Mayo Clinic Alzheimer's Disease Research Center, and the Mayo Clinic Brain Bank. Data collection was supported through funding by NIA grants P50 AG016574, R01 AG032990, U01 AG046139, R01 AG018023, U01 AG006576, U01 AG006786, R01 AG025711, R01 AG017216, R01 AG003949, NINDS grant R01 NS080820, CurePSP Foundation, and support from Mayo Foundation. Study data includes samples collected through the Sun Health Research Institute Brain and Body Donation Program of Sun City, Arizona. The Brain and Body Donation Program is supported by the National Institute of Neurological Disorders and Stroke (U24 NS072026 National Brain and Tissue Resource for Parkinson's Disease and Related Disorders), the National Institute on Aging (P30 AG19610 Arizona Alzheimer's Disease

CoreCenter), the Arizona Department of Health Services (contract 211002, Arizona Alzheimer's Research Center), the Arizona Biomedical Research Commission (contracts 4001, 0011, 05-901 and 1001 to the Arizona Parkinson's Disease Consortium) and the Michael J. Fox Foundation for Parkinson's Research. MSBB data were generated from postmortem brain tissue collected through the Mount Sinai VA MedicalCenter Brain Bank and were provided by Dr. Eric Schadt from Mount Sinai School of Medicine. Mouse RNAseq data from the MODEL-AD consortium is available through Synapse via the AMP-AD knowledge portal (www.synapse.org/#!Synapse:syn17095980)

Authors' contributions

CP designed the novel transcriptome panel and performed bioinformatics analyses. RP, AF, AU, TP performed the gene-expression analyses in human and mouse brain tissue. EP designed the NanoString probes and guided the creation of the novel NanoString panel. BAL and LM curated human brain data. DG, GRH and MS performed mouse experiments. GWC and MS supervised and designed the project. All authors read and approved the manuscript. CP, GWC and RP wrote the manuscript.

Ethics approval

All experiments involving mice were conducted in accordance with policies and procedures described in the Guide for the Care and Use of Laboratory Animals of the National Institutes of Health and were approved by the Institutional Animal Care and Use Committee at The Jackson Laboratory.

Consent for publication

All authors have approved of the manuscript and agree with its submission.

Competing interests

Not applicable

REFERENCES

1. Mayeux R, Stern Y. Epidemiology of Alzheimer disease. Cold Spring Harb Perspect Med [Internet]. 2012 Aug 1 [cited 2019 Jan 14];2(8). Available from: http://www.ncbi.nlm.nih.gov/pubmed/22908189

2. Zhang B, Gaiteri C, Bodea L-G, Wang Z, McElwee J, Podtelezhnikov AA, et al. Integrated systems approach identifies genetic nodes and networks in late-onset Alzheimer's disease. Cell [Internet]. 2013 Apr 25 [cited 2019 Jan 14];153(3):707–20. Available from: http://www.ncbi.nlm.nih.gov/pubmed/23622250

3. Sarah M. Neuner, Timothy J Hohman, Ryan Richholt, David A Bennett, Julie A Schneider, Philip L De Jager, Matthew J Huentelman, Kristen M. S. O'Connell, Catherine C KaczorowskiSarah M. Neuner, Timothy J Hohman, Ryan Richholt, David A Bennett, Julie A Schne CCK. Systems genetics identifies modifiers of Alzheimer's disease risk and resilience. bioRxiv. 2017;

4. Seyfried NT, Dammer EB, Swarup V, Nandakumar D, Duong DM, Yin L, et al. A Multi-network Approach Identifies Protein-Specific Co-expression in Asymptomatic and Symptomatic Alzheimer's Disease. Cell Syst [Internet]. 2017 Jan 25 [cited 2019 Jan 17];4(1):60–72.e4. Available from: http://www.ncbi.nlm.nih.gov/pubmed/27989508

5. Miller JA, Woltjer RL, Goodenbour JM, Horvath S, Geschwind DH. Genes and pathways underlying regional and cell type changes in Alzheimer's disease. Genome Med [Internet]. 2013 [cited 2019 Jan 17];5(5):48. Available from: http://www.ncbi.nlm.nih.gov/pubmed/23705665

6. Matarin M, Salih DA, Yasvoina M, Cummings DM, Guelfi S, Liu W, et al. A Genome-wide Gene-Expression Analysis and Database in Transgenic Mice during Development of Amyloid or Tau Pathology. Cell Rep [Internet]. 2015 Feb 3 [cited 2019 Jan 14];10(4):633–44. Available from: http://www.ncbi.nlm.nih.gov/pubmed/25620700

7. Onos KD, Sukoff Rizzo SJ, Howell GR, Sasner M. Toward more predictive genetic mouse models of Alzheimer's disease. Brain Res Bull [Internet]. 2016 Apr [cited 2019 Jan 14];122:1–11. Available from: http://www.ncbi.nlm.nih.gov/pubmed/26708939

8. Wan Y-W, Al-Ouran R, Mangleburg CG, Lee T V., Allison K, Neuner S, et al. Functional dissection of Alzheimer's disease brain gene expression signatures in humans and mouse models. bioRxiv [Internet]. 2019 Jan 3 [cited 2019 Apr 12];506873. Available from: https://www.biorxiv.org/content/10.1101/506873v1

9. Allen M, Carrasquillo MM, Funk C, Heavner BD, Zou F, Younkin CS, et al. Human whole genome genotype and transcriptome data for Alzheimer's and other neurodegenerative diseases. Sci Data. 2016;3.

10. Jager P De, Ma Y, McCabe C, Xu J, Vardarajan BN, Felsky D, et al. A multi-omic atlas of the human frontal cortex for aging and Alzheimer's disease research. bioRxiv. 2018 Jan;251967.

11. Wang M, Beckmann ND, Roussos P, Wang E, Zhou X, Wang Q, et al. The Mount Sinai cohort of large-scale genomic, transcriptomic and proteomic data in Alzheimer's disease. Sci Data. 2018 Sep;5:180185.

12. Logsdon B, Perumal TM, Swarup V, Wang M, Funk C, Gaiteri C, et al. Meta-analysis of the human brain transcriptome identifies heterogeneity across human AD coexpression modules robust to sample collection and methodological approach. bioRxiv [Internet]. 2019 Jan 3 [cited 2019 Feb 9];510420. Available from: https://www.biorxiv.org/content/10.1101/510420v1

13. Geschwind DH, Rakic P. Cortical evolution: judge the brain by its cover. Neuron [Internet]. 2013 Oct 30 [cited 2019 Apr 10];80(3):633–47. Available from: http://www.ncbi.nlm.nih.gov/pubmed/24183016

14. Bauernfeind AL, Soderblom EJ, Turner ME, Moseley MA, Ely JJ, Hof PR, et al. Evolutionary Divergence of Gene and Protein Expression in the Brains of Humans and Chimpanzees. Genome Biol Evol [Internet]. 2015 Jul 10 [cited 2019 Apr 10];7(8):2276–88. Available from: http://www.ncbi.nlm.nih.gov/pubmed/26163674

15. Rijpma A, Jansen D, Arnoldussen IAC, Fang XT, Wiesmann M, Mutsaers MPC, et al. Sex Differences in Presynaptic Density and Neurogenesis in Middle-Aged ApoE4 and ApoE Knockout Mice. J Neurodegener Dis [Internet]. 2013 [cited 2019 Jan 17];2013:531326. Available from: http://www.ncbi.nlm.nih.gov/pubmed/26316992

16. Siegel JA, Haley GE, Raber J. Apolipoprotein E isoform-dependent effects on anxiety and cognition in female TR mice. Neurobiol Aging [Internet]. 2012 Feb [cited 2019 Jan 17];33(2):345–58. Available from: http://www.ncbi.nlm.nih.gov/pubmed/20400205

17. Allen M, Carrasquillo MM, Funk C, Heavner BD, Zou F, Younkin CS, et al. Human whole genome genotype and transcriptome data for Alzheimer's and other neurodegenerative diseases. Sci Data. 2016 Oct;3:160089.

18. Yu G, Wang L-G, Han Y, He Q-Y. clusterProfiler: an R package for comparing biological themes among gene clusters. OMICS [Internet]. 2012 May [cited 2019 Jun 3];16(5):284–7. Available from: http://www.ncbi.nlm.nih.gov/pubmed/22455463

19. Boyle EI, Weng S, Gollub J, Jin H, Botstein D, Cherry JM, et al. GO::TermFinder--open source software for accessing Gene Ontology information and finding significantly enriched Gene Ontology terms associated with a list of genes. Bioinformatics [Internet]. 2004 Dec 12 [cited 2019 Jun 3];20(18):3710–5. Available from: https://academic.oup.com/bioinformatics/article-lookup/doi/10.1093/bioinformatics/bth456

20. ALTSCHUL SF, GISH W, MILLER W, MYERS EW, LIPMAN DJ. Basic local

alignment search tool. J Mol Biol [Internet]. 1990;215(3):403–10. Available from: http://www.ncbi.nlm.nih.gov/pubmed/2231712

21. Ritchie ME, Phipson B, Wu D, Hu Y, Law CW, Shi W, et al. limma powers differential expression analyses for RNA-Sequencing and microarray studies. Nucleic Acids Res [Internet]. 2015 Apr 20 [cited 2019 Feb 18];43(7):e47–e47. Available from: http://www.ncbi.nlm.nih.gov/pubmed/25605792

22. Bolger AM, Lohse M, Usadel B. Trimmomatic: a flexible trimmer for Illumina sequence data. Bioinformatics [Internet]. 2014 Aug 1 [cited 2019 Jan 17];30(15):2114–20. Available from: http://www.ncbi.nlm.nih.gov/pubmed/24695404

23. Dobin A, Davis CA, Schlesinger F, Drenkow J, Zaleski C, Jha S, et al. STAR: ultrafast universal RNA-Seq aligner. Bioinformatics [Internet]. 2013 Jan 1 [cited 2019 Jan 17];29(1):15–21. Available from: http://www.ncbi.nlm.nih.gov/pubmed/23104886

24. Durinck S, Moreau Y, Kasprzyk A, Davis S, Moor B De, Brazma A, et al. BioMart and Bioconductor: a powerful link between biological databases and microarray data analysis. Bioinformatics [Internet]. 2005 Aug;21(16):3439–40. Available from: http://dx.doi.org/10.1093/bioinformatics/bti525

25. Vilella AJ, Severin J, Ureta-Vidal A, Heng L, Durbin R, Birney E. EnsemblCompara GeneTrees: Complete, duplication-aware phylogenetic trees in vertebrates. Genome Res [Internet]. 2009;19(2):327–35. Available from: http://www.ncbi.nlm.nih.gov/pubmed/19029536

FIGURES

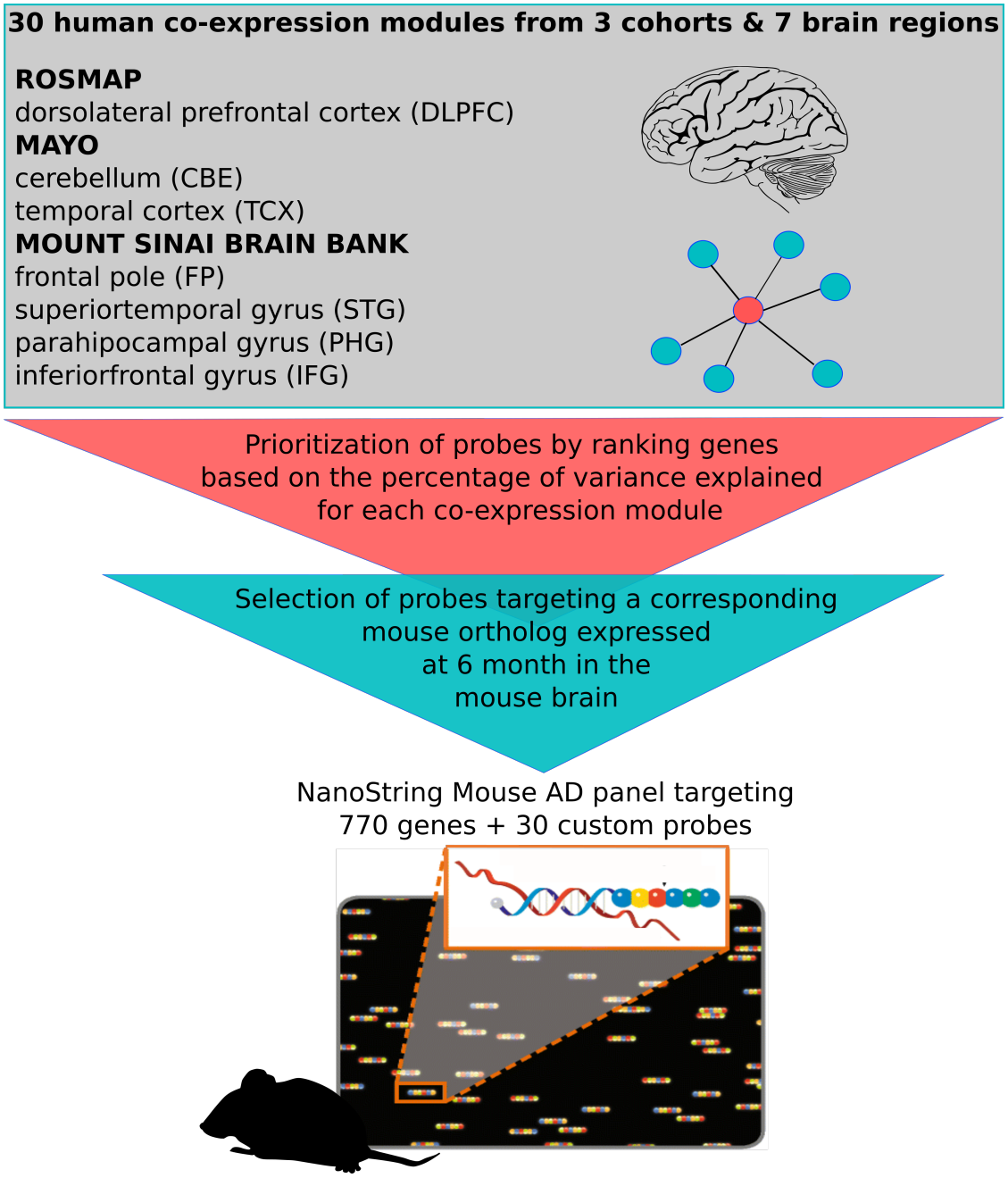

Figure 1: Overview of the nCounter Mouse AD panel design

The novel Mouse AD panel measures expression of genes from a set of 30 human co-expression modules from three human LOAD cohorts, including seven distinct brain regions. Human genes central to each of the human expression modules were prioritized for the Mouse AD panel to select conserved signatures of LOAD associated pathways.

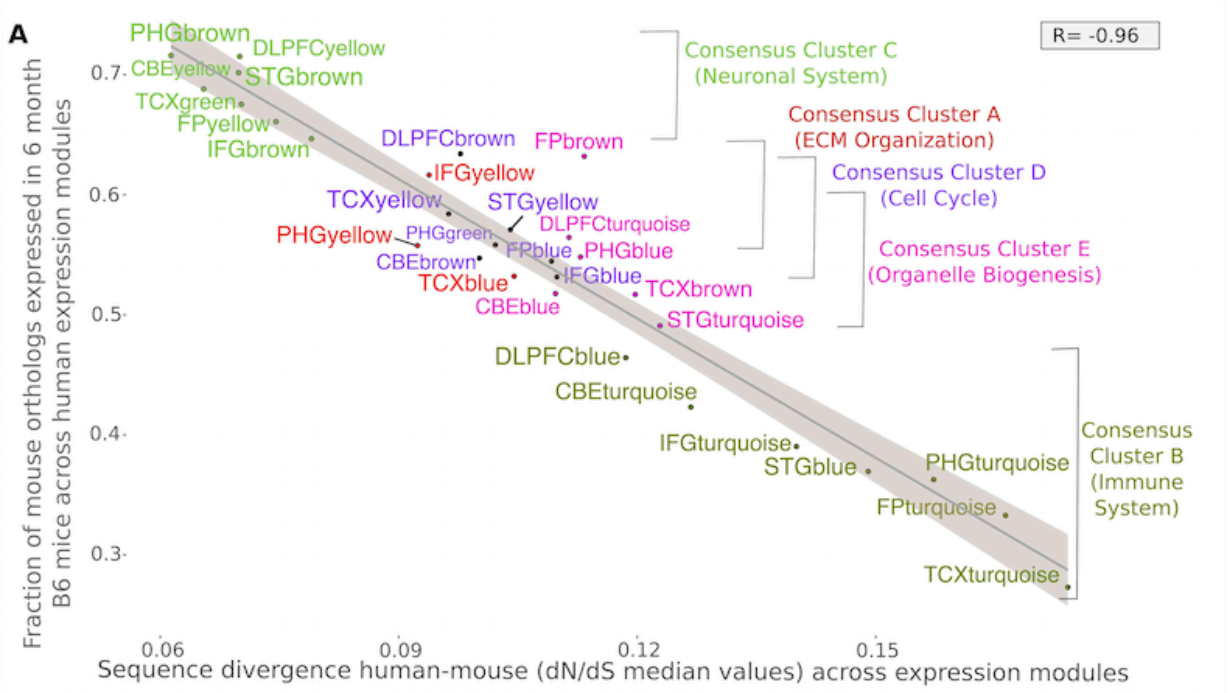

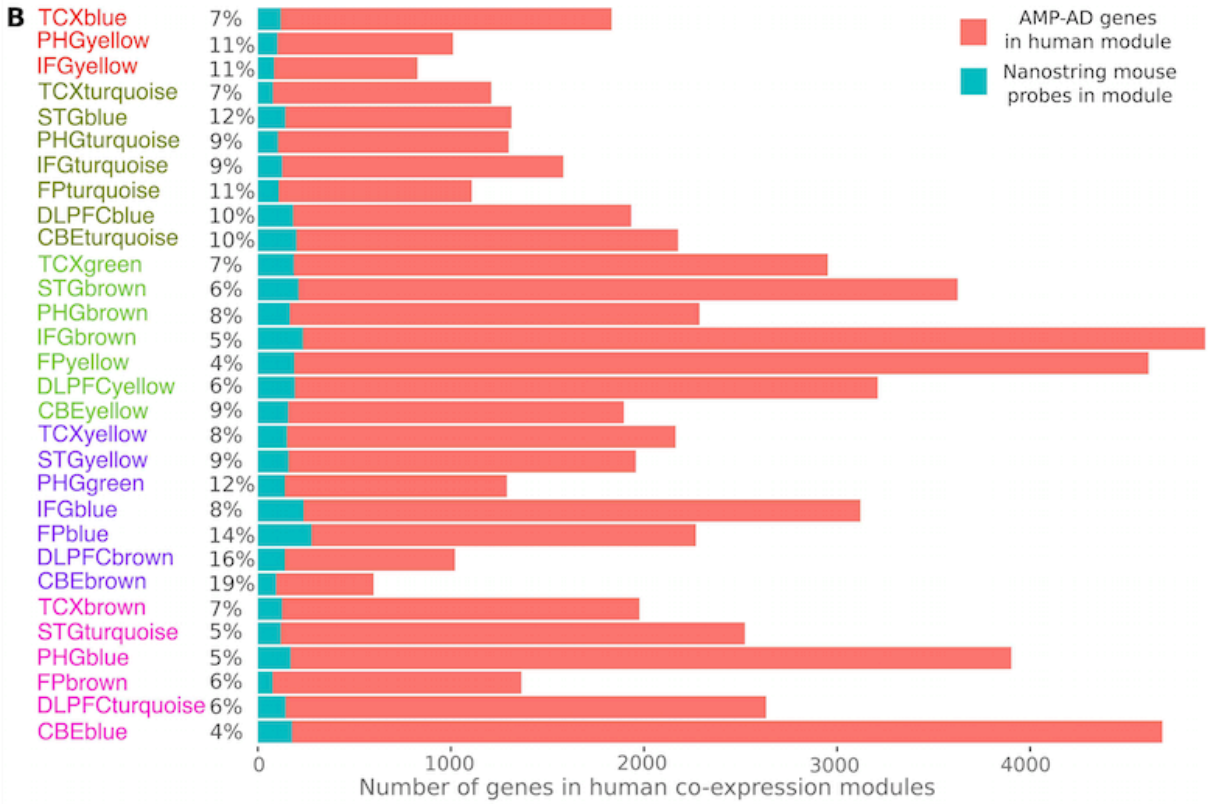

C

	Consensus Cluster A (ECM Organization)	Consensus Cluster B (Immune System)	Consensus Cluster C (Neuronal System)	Consensus Cluster D (Cell Cycle)	Consensus Cluster E (Organelle Biogenesis)
Genes in Modules (Median)	743-1713 (910)	1001-1977 (1195)	1739-4673 (3019)	504-1991 (1799)	1289-4509 (2447)
% Probe Coverage (Median)	7-11% (11%)	7-12% (10%)	4-9% (6%)	8-19% (12%)	4-7% (6%)

Figure 2: Human to mouse comparison and probe coverage summary statistics

(A) Human-mouse sequence divergence (median dN/dS values) is inversely correlated (Pearson's correlation coefficient: -0.96) with the fraction of genes being expressed in B6 mouse brain for each of the human co-expression modules. **(B)** Coverage of the 770 selected mouse NanoString probes for the 30 human co-expression modules associated with five functional consensus clusters. The size and number of human co-expression modules differs for the three post-mortem brain cohorts (ROSMAP, Mayo, Mount Sinai Brain Bank) and across the seven included brain regions. (**C**) This results in a varying degree of probe coverage for each module with a number of disease associated consensus clusters (A-E), reflecting disease related pathways and processes.

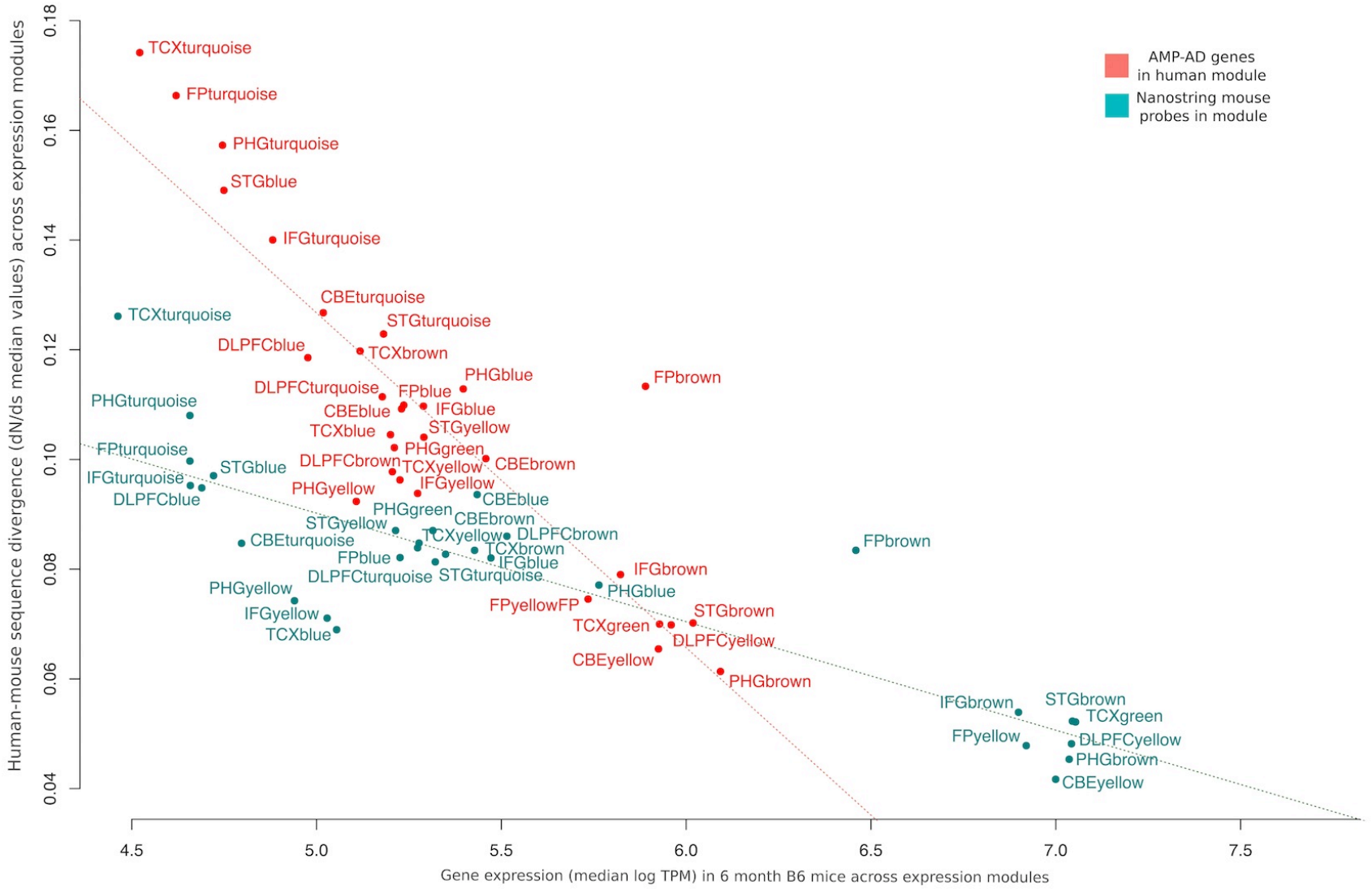
AMP-AD genes
in human module
Nanostring mouse
probes in module
Human-mouse sequence divergence (dN/ds median values) across expression modules
0.04
0.06
0.08
0.10
0.12
0.14
0.16
0.18
4.5
5.0
5.5
6.0
6.5
7.0
7.5
Gene expression (median log TPM) in 6 month B6 mice across expression modules
TCXturquoise
FPturquoise
PHGturquoise
STGblue
IFGturquoise
CBEturquoise
STGturquoise
DLPFCblue
TCXbrown
PHGblue
FPbrown
DLPFCturquoise
FPblue
IFGblue
CBEblue
STGyellow
TCXblue
PHGgreen
DLPFCbrown
TCXyellow
CBEbrown
IFGyellow
PHGyellow
CBEblue
PHGgreen
CBEbrown
STGyellow
TCXyellow
DLPFCbrown
CBEturquoise
TCXbrown
IFGblue
FPblue
DLPFCturquoise
STGturquoise
IFGbrown
PHGblue
PHGyellow
FPyellowFP
STGbrown
IFGyellow
TCXgreen
DLPFCyellow
TCXblue
CBEyellow
PHGbrown
IFGbrown
STGbrown
TCXgreen
FPyellow
DLPFCyellow
PHGbrown
CBEyellow

Figure 3: NanoString Mouse AD probe genes are more conserved and have greater expression in the mouse brain

Comparison between gene-level sequence divergence and transcript abundances in six month old B6 mouse brains for all genes (red) and the subset of 770 genes covered by NanoString probes (green).

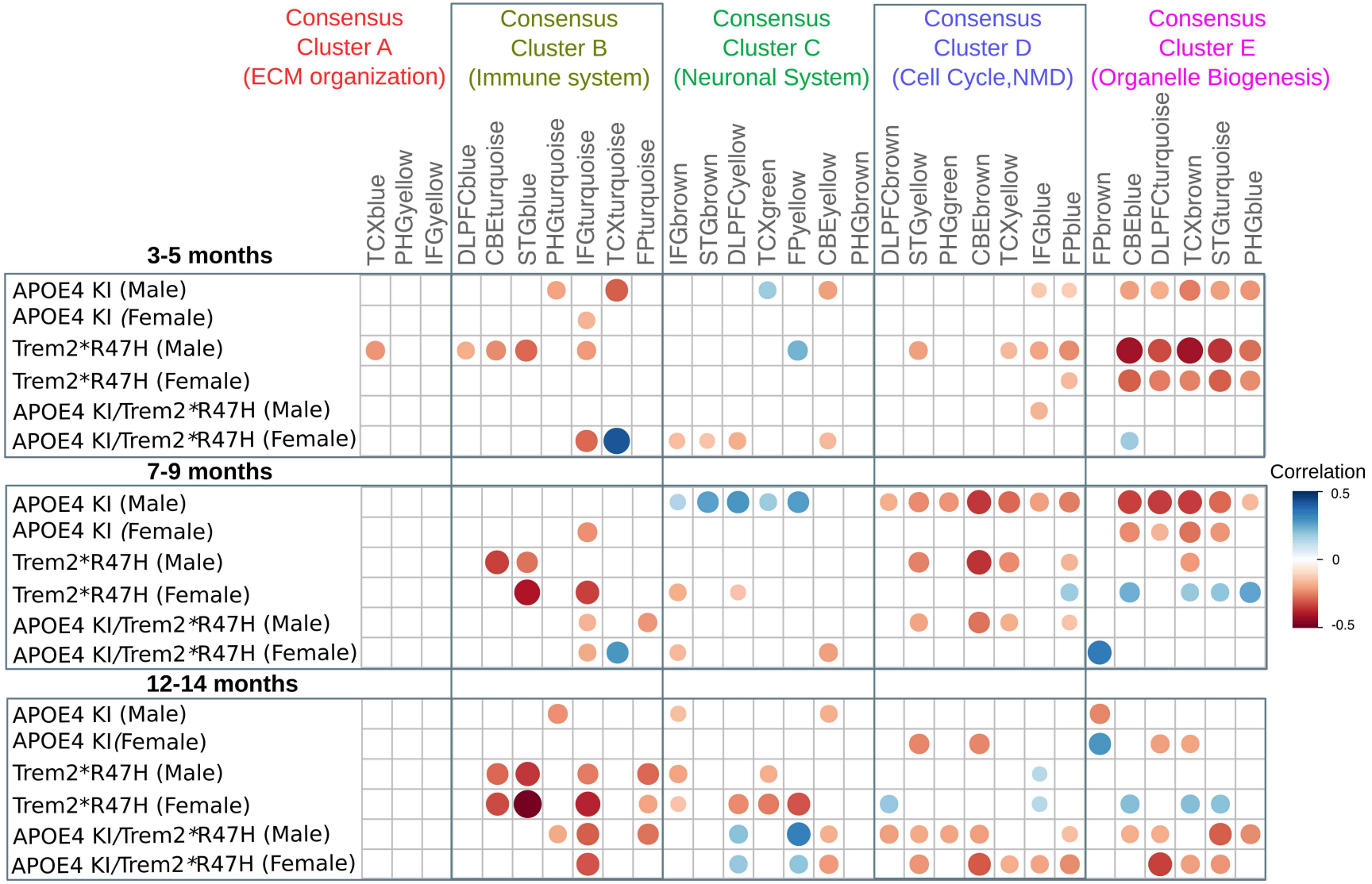
Consensus Cluster A (ECM organization)
Consensus Cluster B (Immune system)
Consensus Cluster C (Neuronal System)
Consensus Cluster D (Cell Cycle,NMD)
Consensus Cluster E (Organelle Biogenesis)
TCXblue
PHGyellow
IFGyellow
DLPFCblue
CBEturquoise
STGblue
PHGturquoise
IFGturquoise
TCXturquoise
FPturquoise
IFGbrown
STGbrown
DLPFCyellow
TCXgreen
FPyellow
CBEyellow
PHGbrown
DLPFCbrown
STGyellow
PHGgreen
CBEbrown
TCXyellow
IFGblue
FPblue
FPbrown
CBEblue
DLPFCturquoise
TCXbrown
STGturquoise
PHGblue
3-5 months
APOE4 KI (Male)
APOE4 KI (Female)
Trem2*R47H (Male)
Trem2*R47H (Female)
APOE4 KI/Trem2*R47H (Male)
APOE4 KI/Trem2*R47H (Female)
7-9 months
APOE4 KI (Male)
APOE4 KI (Female)
Trem2*R47H (Male)
Trem2*R47H (Female)
APOE4 KI/Trem2*R47H (Male)
APOE4 KI/Trem2*R47H (Female)
12-14 months
APOE4 KI (Male)
APOE4 KI (Female)
Trem2*R47H (Male)
Trem2*R47H (Female)
APOE4 KI/Trem2*R47H (Male)
APOE4 KI/Trem2*R47H (Female)
Correlation
0.5
0
-0.5

Figure 4: Correlations between mouse model effects and LOAD effects for the NanoString Mouse AD panel genes across 30 human co-expression modules

Circles correspond to significant (p-value < 0.05) positive (blue) and negative (red) Pearson's correlation coefficients for gene expression changes in mice (log fold change of strain minus age-matched B6 mice) and human disease (log fold change for cases minus controls). Human co-expression modules are ordered into Consensus Clusters A-E (12) describing major sources of AD-related alterations in transcriptional states across independent studies and brain regions. Consensus clusters are annotated based on the most significantly enriched and non-redundant Reactome pathway terms (Supplemental Tables S1, S2).

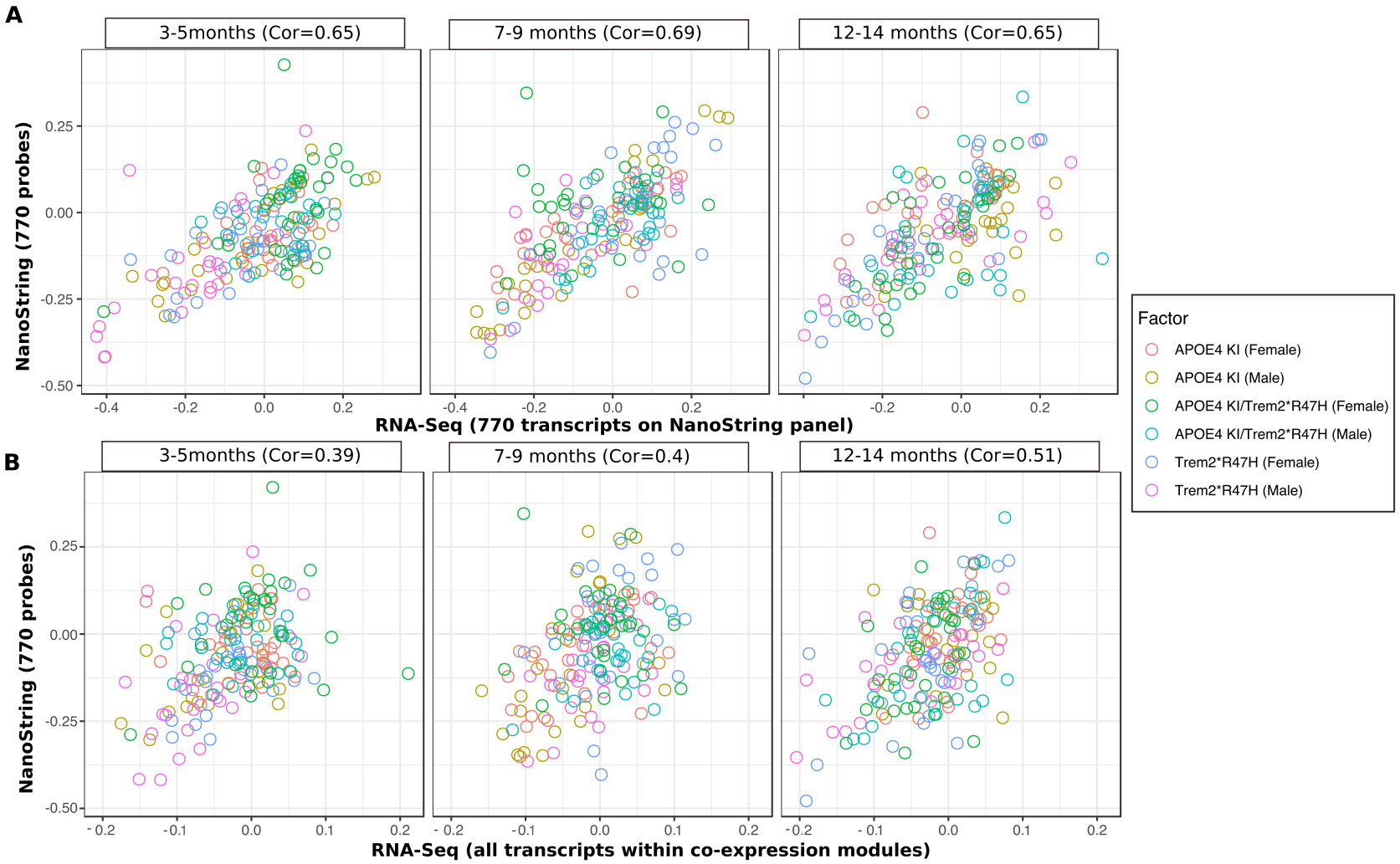
A
3-5months (Cor=0.65)
7-9 months (Cor=0.69)
12-14 months (Cor=0.65)
NanoString (770 probes)
RNA-Seq (770 transcripts on NanoString panel)
B
3-5months (Cor=0.39)
7-9 months (Cor=0.4)
12-14 months (Cor=0.51)
NanoString (770 probes)
RNA-Seq (all transcripts within co-expression modules)
Factor
APOE4 KI (Female)
APOE4 KI (Male)
APOE4 KI/Trem2*R47H (Female)
APOE4 KI/Trem2*R47H (Male)
Trem2*R47H (Female)
Trem2*R47H (Male)

Figure 5: Platform comparison between the nCounter Mouse AD panel and RNA-Seq correlation with AMP-AD modules across 137 samples

The plots display the correlation between human AMP-AD co-expression modules and gene expression profiles derived from the NanoString panel and RNA-Seq data for the same 137 mouse samples. A detailed comparison is provided for three different age stages and three mouse models carrying LOAD associated risk variants. **(A)** A strong positive correlation was observed across all ages and samples combined when comparing expression of the 770 transcripts on the NanoString panel. **(B)** The correlation between NanoString and RNA-Seq expression analysis decreased overall when comparing all module transcripts measured by RNA-Seq to the subset of 770 probes on the NanoString panel. However, an age specific effect was observed for the mouse transcripts in which correlation with human co-expression modules increased with age.